INTERNATIONAL JOURNAL FOR NUMERICAL METHODS IN FLUIDS
Int. J. Numer. Meth. Fluids 2010; **62**:166–187
Published online 20 February 2009 in Wiley InterScience (www.interscience.wiley.com). DOI: 10.1002/fld.2010

New stabilized finite element method for time-dependent incompressible flow problems

Yueqiang Shang[1, 2, *, †]

[1]*Faculty of Science, Xi'an Jiaotong University, Xi'an 710049, People's Republic of China*
[2]*School of Mathematics and Computer Science, Guizhou Normal University, Guiyang 550001, People's Republic of China*

SUMMARY

A new stabilized finite element method is considered for the time-dependent Stokes problem, based on the lowest-order $P_1 - P_0$ and $Q_1 - P_0$ elements that do not satisfy the discrete *inf–sup* condition. The new stabilized method is characterized by the features that it does not require approximation of the pressure derivatives, specification of mesh-dependent parameters and edge-based data structures, always leads to symmetric linear systems and hence can be applied to existing codes with a little additional effort. The stability of the method is derived under some regularity assumptions. Error estimates for the approximate velocity and pressure are obtained by applying the technique of the Galerkin finite element method. Some numerical results are also given, which show that the new stabilized method is highly efficient for the time-dependent Stokes problem. Copyright © 2009 John Wiley & Sons, Ltd.

Received 26 June 2008; Revised 29 December 2008; Accepted 7 January 2009

KEY WORDS: time-dependent incompressible flow; Stokes equations; finite element method; stabilized method; stability analysis; error estimate

1. INTRODUCTION

The development of efficient finite element methods for the Stokes equations and the Navier–Stokes equations is a key component in incompressible flow simulations. By the use of a primitive-variable formulation, the importance of ensuring the compatibility of the approximations for the velocity and the pressure by satisfying the so-called *inf–sup* condition is widely understood. However, various simple mixed elements like the lowest-order $P_1 - P_0$ (linear velocity, constant

*Correspondence to: Yueqiang Shang, Faculty of Science, Xi'an Jiaotong University, P.O. Box 2325, Xi'an 710049, People's Republic of China.
†E-mail: yueqiangshang@gmail.com

Contract/grant sponsor: The Science and Technology Foundation of Guizhou Province, China; contract/grant number: [2008]2123

pressure) triangular element and $Q_1 - P_0$ (bilinear velocity, constant pressure) quadrilateral element not satisfying the *inf–sup* condition may also work well by using the stabilized finite element methods.

For these lowest-order elements not satisfying the *inf–sup* condition, various stabilized techniques have been proposed and studied. Some of these stabilized techniques belong to the class of residual-based methods or are closely related to residual-based stabilized methods; for example, the stream upwind Petrov–Galerkin (SUPG) method [1, 2], the Brezzi–Pitkaranta method [3], the Douglas–Wang method [4], the well-known Galerkin least squares (GLS) method [5–7], the method of bubble function enrichment [8, 9], the related unusual stabilized methods [10] and the recent methods arising from the enrichment of the finite element space by multiscale functions [11, 12] (see [13] for a review on these methods). Most of these residual-based methods necessarily introduce stabilization parameters either explicitly or implicitly which, in practice, are still being determined by trial and error. Moreover, there is no satisfactory answer to the stabilized parameters in all situations. Therefore, the development of mixed finite elements free from stabilization parameters has become increasingly important.

On the other hand, there are some stabilized mixed finite element methods involving non-residual stabilization. Examples include the pressure gradient projection (PGP) method [14–16], the related local pressure gradient stabilization (LPS) method [17] in which the incompressibility constraint is relaxed by subtracting the discontinuous pressure gradient from its projection onto a piecewise polynomial space, and the local and global pressure jump formulations [18–20] where the continuity equation is relaxed using the jumps of pressure across the interelement interfaces. However, it is clear that both PGP and LPS methods are not appropriate for pairs with constant pressure elements, while the local and global pressure jump formulations require edge-based data structures and a subdivision of grids into patches.

Some of the above techniques have also been extended to transient incompressible flow problems. For example, the SUPG formulation has been extended to the transient Navier–Stokes equations in [21, 22]; the GLS method has been studied and compared with the characteristic-based split method for the time-dependent Navier–Stokes equations [23] and the Brezzi–Pitkaranta technique has been studied for the transient Stokes problem [24]. In [25], combining implicit time integration with stabilized spatial discretization, Bochev, Gunzburger and Shadid have studied and compared three stabilization methods (namely, GLS, Douglas–Wang and Brezzi–Pitkaranta) for the transient Stokes problem. In [26], the bubble enrichment stabilized method has been studied for the transient Stokes problem. Depending on whether bubbles are allowed to evolve with time or they are considered quasi-static, the authors derived two different methods. Using a macroelement technique, He *et al.* have studied a fully discrete stabilized $P_1 - P_0$ and $Q_1 - P_0$ finite element solution to the time-dependent Navier–Stokes equations based on the backward Euler and Crank–Nicolson extrapolation schemes of time discretization in [27, 28], respectively. Based on two local Gauss integrations, a new stabilized finite element method has been proposed and compared numerically with other methods (standard Galerkin, penalty, GLS and multiscale enrichment) for the transient Navier–Stokes equations by using the lowest equal-order pair of finite elements in [29]. We refer the reader, for example, to [30–32] and the references therein for other stabilized methods for the transient incompressible flow problems.

Recently, based on polynomial pressure projection, a new family of stabilized methods for the stationary Stokes equations has been proposed and studied in [33, 34]. Based on a detailed study of the instabilities of the lowest-order velocity–pressure pairs, these new methods add terms

DOI: 10.1002/fld

to the continuity equation particularly suited to stabilize these instabilities. These added terms depend on the projection operators of pressure whose actions can be evaluated locally at the element level using the standard finite element techniques. The new family of stabilized methods is characterized by the following features. First, the methods do not require approximation of the pressure derivatives, specification of mesh-dependent parameters and edge-based data structures. Second, the methods are unconditionally stable, optimally accurate, parameter-free, and always lead to symmetric linear systems. Consequently, the new stabilized methods can be applied to existing codes with a little additional effort. Based on two local Gauss integrations, a similar parameter-free stabilized finite element method has also been proposed for the steady Stokes and Navier–Stokes equations in [35, 36], respectively, in the context of the lowest equal-order P_1-P_1 and Q_1-Q_1 elements. Unfortunately, this stabilized method does not work for the P_1-P_0 or Q_1-P_0 element.

This paper aims to extend the work of Bochev *et al.* [33, 34] to the two-dimensional time-dependent Stokes problem. We only confine our attention to the P_1-P_0 triangular element and the Q_1-P_0 quadrilateral element in the theoretical analysis. However, for comparison, numerical results for the lowest equal-order P_1-P_1 triangular element and the stable MIN element are also given. Following the abstract framework of Li *et al.* [29], we first define the stabilized method for the lowest-order conforming P_1-P_0 and Q_1-P_0 elements, then show their well-posedness and derive the error estimates. Our theoretical results are similar to that in [29]. However, this paper is different from [29] due to that they use different stabilization methods to stabilize different elements for different equations. The main work of this paper is to use the pressure projection technique to stabilize the lowest-order conforming P_1-P_0 and Q_1-P_0 elements for which the stabilization technique proposed in [29] (i.e. using the difference between a consistent and an under-integrated mass matrices computed by two different-order local Gauss integrations to offset the *inf–sup* condition) does not work. Although we also give the numerical results for the P_1-P_1 element, we use a naturally different pressure projection operator from that in [29]. Therefore, this paper can be considered as a sequel of the work of Bochev *et al.* in [33, 34] and a complement to the work of [29] in the sense that it demonstrates the high efficiency of the local pressure projection stabilized methods not only for the steady problems, but also for the unsteady problems and illustrates the great flexibility of the definition of the pressure projection operator.

The remainder of this paper is organized as follows. In the next section, some basic notations and preliminary results for the time-dependent Stokes problem are stated. In Section 3, the stabilized finite element method is introduced. Stability and error estimates for the stabilized finite element solution are derived in Section 4. In Section 5, some numerical results are given to illustrate the theoretical results. Finally, some conclusion are drawn in Section 6.

2. PRELIMINARIES

Let Ω be a bounded domain with Lipschitz-continuous boundary $\partial\Omega$ in R^2. We shall use the standard notation for Sobolev spaces $W^{s,p}(\Omega)$, $W^{s,p}(\Omega)^2$ and their associated norms and seminorms; see, e.g. [37, 38]. For $p=2$, we denote $H^s(\Omega)=W^{s,2}(\Omega)$, $H^s(\Omega)^2=W^{s,2}(\Omega)^2$ and $H_0^1(\Omega)=\{v\in H^1(\Omega): v|_{\partial\Omega}=0\}$, where $v|_{\partial\Omega}=0$ is in the sense of trace, $\|\cdot\|_{s,\Omega}=\|\cdot\|_{s,2,\Omega}$. Owing to the norm equivalence between $\|u\|_1$ and $\|\nabla u\|_0$ on $H_0^1(\Omega)$, we use the same notation for them in this paper.

DOI: 10.1002/fld

We consider the time-dependent incompressible Stokes problem in R^2

$$\begin{aligned} u_t - \nu\Delta u + \nabla p &= f \quad \text{in } \Omega\times(0,T] \\ \operatorname{div} u &= 0 \quad \text{in } \Omega\times(0,T] \\ u &= 0 \quad \text{on } \partial\Omega\times(0,T] \\ u &= u_0 \quad \text{on } \Omega\times\{0\} \end{aligned} \tag{1}$$

where $u=u(x,t)=(u_1(x,t),u_2(x,t))$ is the velocity, $p=p(x,t)$ the pressure, $f=f(x,t)$ the prescribed body force, $\nu>0$ the viscosity, u_0 the initial velocity, T the given final time and $u_t=\partial u/\partial t$. We assume that the data (u_0, f) satisfy the assumption:

A0. $u_0\in H^2(\Omega)^2\cap H_0^1(\Omega)^2$ with $\operatorname{div} u_0=0$ and $f,\ f_t\in L^2(0,T;L^2(\Omega)^2)$ with

$$\|u_0\|_2+\left(\int_0^T(\|f\|_0^2+\|f_t\|_0^2)\,\mathrm{d}t\right)^{1/2}\leqslant c \tag{2}$$

Here and hereafter, we use the letter c to denote a generic positive constant which is independent of the mesh parameter, while it may depend on the data (ν,Ω,u_0,f,T) and stand for different values at its different occurrences.

For a given function $f\in L^2(0,T;L^2(\Omega)^2)$, the variational formulation of problem (1) reads: Find a pair of $(u,p)\in L^2(0,T;H_0^1(\Omega)^2)\times L^2(0,T;L_0^2(\Omega))$ such that

$$(u_t,v)+B((u,p);(v,q))=(f,v)\quad \forall(v,q)\in H_0^1(\Omega)^2\times L_0^2(\Omega) \tag{3}$$

$$u(0)=u_0 \tag{4}$$

where

$$L_0^2(\Omega)=\left\{q\in L^2(\Omega):\int_\Omega q\,\mathrm{d}x=0\right\}$$

$(\cdot,\cdot)$ denotes the standard inner-product of $L^2(\Omega)$, the bilinear form B is defined as

$$B((u,p);(v,q))=a(u,v)-d(v,p)+d(u,q)$$

and

$$a(u,v)=\nu(\nabla u,\nabla v),\quad d(v,q)=(\operatorname{div} v,q)\quad \forall u,v\in H_0^1(\Omega)^2,\ \ q\in L_0^2(\Omega)$$

As for the existence, uniqueness and regularity of a global strong solution to the time-dependent Stokes problems, we have the following results [39]:

Lemma 1

Assume that $\partial\Omega$ is of C^2 or Ω is a two-dimensional bounded convex polygon and A0 hold, then for any given function $f\in L^2(0,T;L^2(\Omega)^2)$, problem (1) admits a unique solution (u,p) satisfying the following regularities:

$$\sup_{0<t\leqslant T}(\|u_t(t)\|_0^2+\|u(t)\|_2^2+\|p(t)\|_1^2)\leqslant c \tag{5}$$

$$\sup_{0<t\leqslant T}\sigma(t)\|u_t(t)\|_1^2+\int_0^T\sigma(t)(\|u_{tt}(t)\|_0^2+\|u_t(t)\|_2^2+\|p_t(t)\|_1^2)\,\mathrm{d}t\leqslant c \tag{6}$$

DOI: 10.1002/fld

where $\sigma(t)=\min\{1,t\}$ whose appearance in (6) is due to the non-smoothness of the time derivations of the velocity u and the pressure p at $t=0$.

3. STABILIZED FINITE ELEMENT METHOD

Assume $T^h(\Omega)=\{K\}$ be a regular triangulation (see, e.g. [40, 41]) of Ω into triangles or quadrilaterals with mesh size $h>0$. Associated with the mesh $T^h(\Omega)$, the finite element subspaces of interest in this paper are defined by

$$R_1(K)=\begin{cases} P_1(K) & \text{if } K \text{ is triangular} \\ Q_1(K) & \text{if } K \text{ is quadrilateral} \end{cases} \tag{7}$$

giving the continuous piecewise (bi)linear velocity subspace

$$X_h=\{v_h\in H_0^1(\Omega)^2 : v_h|_K\in R_1(K)^2 \ \forall K\in T^h(\Omega)\}$$

and the piecewise constant pressure subspace

$$M_h=\{q_h\in L_0^2(\Omega) : q_h|_K\in P_0(K) \ \forall K\in T^h(\Omega)\}$$

It is noted that neither of these methods is stable in the standard Babuška–Brezzi sense; P_1-P_0 triangle 'lock' on regular grids (since there are more discrete incompressibility constraints than velocity degrees of freedom), and the Q_1-P_0 quadrilateral is the most infamous example of an unstable mixed method, as elucidated by Sani *et al.* [42].

Introducing the following pressure projection operator (see [33, 34])

$$\Pi: L^2(\Omega)\to R_1 \tag{8}$$

having a continuous range and the following properties

$$(p,q_h)=(\Pi p,q_h) \quad \forall p\in L^2(\Omega), \ \ q_h\in R_1 \tag{9}$$

$$\|\Pi p\|_0\leqslant c\|p\|_0 \quad \forall p\in L^2(\Omega) \tag{10}$$

$$\|p-\Pi p\|_0\leqslant ch\|p\|_1 \quad \forall p\in H^1(\Omega) \tag{11}$$

we derive the stabilized finite element formulation of problem (3)–(4): Find $(u_h(t), p_h(t))\in X_h\times M_h$, $t\in[0,T]$, such that

$$(u_{ht},v_h)+\mathscr{B}((u_h,p_h);(v_h,q_h))=(f,v_h) \quad \forall (v_h,p_h)\in X_h\times M_h \tag{12}$$

$$u_h(0)=u_{0h} \tag{13}$$

where u_{0h} is an approximation of u_0,

$$\mathscr{B}((u_h,p_h);(v_h,q_h))=B((u_h,p_h);(v_h,q_h))+\mathscr{C}(p_h,q_h)$$

is the new stabilized bilinear form and $\mathscr{C}(\cdot,\cdot)$ is the stabilization term (see [33, 34]) defined by

$$\mathscr{C}(p,q)=((I-\Pi)p,(I-\Pi)q) \quad \forall p,q\in L^2(\Omega) \tag{14}$$

The following theorem establishes the weak coercivity of the bilinear form $\mathscr{B}((u,p);(v,q))$ for the lowest-order finite element pairs.

DOI: 10.1002/fld

Theorem 1 (*Bochev et al.* [*33*])
Let (X_h, M_h) be defined as above. Then there exists a positive constant β, independent of h, such that

$$|\mathscr{B}((u,p);(v,q))|\leqslant c(\|u\|_1+\|p\|_0)(\|v\|_1+\|q\|_0) \quad \forall (u,p),(v,q)\in H_0^1(\Omega)^2\times L_0^2(\Omega) \tag{15}$$

$$\beta(\|u_h\|_1+\|p_h\|_0)\leqslant \sup_{(v_h,q_h)\in X_h\times M_h}\frac{|\mathscr{B}((u_h,p_h);(v_h,q_h))|}{\|v_h\|_1+\|q_h\|_0} \quad \forall (u_h,p_h)\in X_h\times M_h \tag{16}$$

4. STABILITY ANALYSIS AND ERROR ESTIMATES

We first define a projection operator $(R_h, Q_h): H_0^1(\Omega)^2\times L_0^2(\Omega)\to X_h\times M_h$ by

$$\begin{aligned}&\mathscr{B}((R_h(v,q),Q_h(v,q));(v_h,q_h))=B((v,q);(v_h,q_h))\\ &\forall (v,q)\in H_0^1(\Omega)^2\times L_0^2(\Omega),\quad (v_h,q_h)\in X_h\times M_h\end{aligned} \tag{17}$$

Note that due to Theorem 1, (R_h, Q_h) is well defined and satisfies the following approximate properties:

Lemma 2 (*Li et al.* [*29*])
Under the assumptions of Lemma 1 and Theorem 1, the projection operator (R_h, Q_h) satisfies

$$\|v-R_h(v,q)\|_1+\|q-Q_h(v,q)\|_0\leqslant c(\|v\|_1+\|q\|_0) \tag{18}$$

for all $(v,q)\in H_0^1(\Omega)^2\times L_0^2(\Omega)$ and

$$\|v-R_h(v,q)\|_0+h(\|v-R_h(v,q)\|_1+\|q-Q_h(v,q)\|_0)\leqslant ch^2(\|v\|_2+\|q\|_1) \tag{19}$$

for all $(v,q)\in D(A)\times(H^1(\Omega)\cap L_0^2(\Omega))$, where $D(A)=\{v\in H^2(\Omega)^2\cap H_0^1(\Omega)^2:\operatorname{div} v=0\}$.

Owing to $u_0\in D(A)$, we can define $p_0\in H^1(\Omega)\cap L_0^2(\Omega)$ [39], then define $(u_{0h},p_{0h})=(R_h(u_0,p_0),Q_h(u_0,p_0))$. Further, we set $(e_h,\eta_h)=(R_h(u,p)-u_h,Q_h(u,p)-p_h)$, $(\mathscr{E},\mathscr{F})=(u-R_h(u,p),p-Q_h(u,p))$ and $(e,\eta)=(u-u_h,p-p_h)=(e_h+\mathscr{E},\eta_h+\mathscr{F})$. From Lemma 1 and (19), we have, for $t\in[0,T]$,

$$\|\mathscr{E}\|_0+h\|\mathscr{E}\|_1\leqslant ch^2,\quad \int_0^t\sigma(s)\|\mathscr{E}_t\|_0^2\,\mathrm{d}s\leqslant ch^4 \tag{20}$$

4.1. Stability analysis

Theorem 2
Under the assumptions of Lemma 1 and Theorem 1, the solution (u_h, p_h) of (12) and (13) satisfies

$$\|u_h(t)\|_0^2+\int_0^t(\nu\|u_h\|_1^2+\|p_h\|_0^2+\|u_{ht}\|_0^2)\,\mathrm{d}s\leqslant c \tag{21}$$

for all $t\in[0,T]$.

DOI: 10.1002/fld

Proof

Taking $(v, q)=(u_h, p_h)$ in (12) and using the Schwarz, Poincaré and Young inequalities, we have

$$\frac{1}{2}\frac{\mathrm{d}}{\mathrm{d}t}\|u_h\|_0^2+\nu\|u_h\|_1^2+\mathscr{C}(p_h, p_h)\leqslant\frac{1}{2}\nu\|u_h\|_1^2+\frac{1}{2}\nu^{-1}C_\Omega^2\|f\|_0^2 \tag{22}$$

where C_Ω is the constant of the Poincaré inequality. Integrating (22) over $[0, t]$ and noting that

$$\|u_{0h}\|_0=\|R_h(u_0, p_0)\|_0\leqslant\|u_0\|_0+\|u_0-R_h(u_0, p_0)\|_0\leqslant c(\|u_0\|_1+\|p_0\|_0)$$

we obtain

$$\|u_h(t)\|_0^2+\int_0^t(\nu\|u_h\|_1^2+2\mathscr{C}(p_h, p_h))\,\mathrm{d}s\leqslant c \tag{23}$$

Combining (16) with (12), and using the Schwarz and Poincaré inequalities, we get

$$\begin{aligned}\beta(\|u_h\|_1+\|p_h\|_0)&\leqslant\sup_{(v_h,q_h)\in X_h\times M_h}\frac{|\mathscr{B}((u_h, p_h); (v_h, q_h))|}{\|v_h\|_1+\|q_h\|_0}\\&=\sup_{(v_h,q_h)\in X_h\times M_h}\frac{|(f, v_h)-(u_{ht}, v_h)|}{\|v_h\|_1+\|q_h\|_0}\\&\leqslant\sup_{(v_h,q_h)\in X_h\times M_h}\frac{C_\Omega(\|f\|_0+\|u_{ht}\|_0)\|v_h\|_1}{\|v_h\|_1+\|q_h\|_0}\\&\leqslant C_\Omega(\|f\|_0+\|u_{ht}\|_0)\end{aligned}$$

which yields

$$\|p_h\|_0^2\leqslant\frac{2C_\Omega^2}{\beta^2}(\|f\|_0^2+\|u_{ht}\|_0^2)$$

Integrating the above inequality from 0 to t, we find

$$\int_0^t\|p_h\|_0^2\,\mathrm{d}s\leqslant\frac{2C_\Omega^2}{\beta^2}\int_0^t(\|f\|_0^2+\|u_{ht}\|_0^2)\,\mathrm{d}s \tag{24}$$

We now estimate $\int_0^t\|u_{ht}\|_0^2\,\mathrm{d}s$. By differentiating the term $d(u_h, q_h)+\mathscr{C}(p_h, q_h)$ with respect to t in (12), then setting $(v_h, q_h)=(u_{ht}, p_h)$, one gets

$$\|u_{ht}\|_0^2+\frac{1}{2}\frac{\mathrm{d}}{\mathrm{d}t}(\nu\|u_h\|_1^2+\mathscr{C}(p_h, p_h))=(f, u_{ht})\leqslant\frac{1}{2}\|f\|_0^2+\frac{1}{2}\|u_{ht}\|_0^2$$

Integrating the above inequality over $[0, t]$, using (2) and noting that

$$\|u_{0h}\|_1^2\leqslant\|u_0\|_1^2+\|u_0-R_h(u_0, p_0)\|_1^2\leqslant c(\|u_0\|_1^2+\|p_0\|_0^2)$$

and

$$\mathscr{C}(p_{0h}, p_{0h})\leqslant c\|p_{0h}\|_0^2\leqslant c(\|p_0\|_0^2+\|p_0-Q_h(u_0, p_0)\|_0^2)\leqslant c(\|u_0\|_1^2+\|p_0\|_0^2)$$

DOI: 10.1002/fld

we obtain

$$\int_0^t \|u_{ht}\|_0^2 \,\mathrm{d}s + \nu\|u_h(t)\|_1^2 + \mathscr{C}(p_h(t), p_h(t)) \leqslant c \tag{25}$$

Combining (25) with (24), (23) and (2), we complete the proof of (21). □

4.2. Error estimates

This subsection is devoted to the H^1-error estimate of the discrete velocity u_h and the L^2-error estimate of the discrete pressure.

Lemma 3
Under the conditions of Lemma 1 and Theorem 1, it holds that, for $t \in [0, T]$,

$$\|u(t) - u_h(t)\|_0^2 + \int_0^t (\nu\|u - u_h\|_1^2 + \mathscr{C}(p - p_h, p - p_h))\,\mathrm{d}s \leqslant ch^2 \tag{26}$$

Proof
Subtracting (12) from (3) with $(v, q) = (v_h, q_h)$, we find that

$$(u_t - u_{ht}, v_h) + \mathscr{B}((u - u_h, p - p_h); (v_h, q_h)) = \mathscr{C}(p, q_h) \quad \forall (v_h, q_h) \in X_h \times M_h \tag{27}$$

which, together with (17), yields

$$(u_t - u_{ht}, v_h) + \mathscr{B}((e_h, \eta_h); (v_h, q_h)) = 0 \quad \forall (v_h, q_h) \in X_h \times M_h \tag{28}$$

Setting $(v_h, q_h) = (e_h, \eta_h)$ in (28), we deduce

$$(u_t - u_{ht}, e_h) + \nu\|e_h\|_1^2 + \mathscr{C}(\eta_h, \eta_h) = 0$$

Noting $u - u_h = e_h + \mathscr{E}$ and using (19), we obtain

$$\begin{aligned} \frac{1}{2}\frac{\mathrm{d}}{\mathrm{d}t}\|u - u_h\|_0^2 + \nu\|e_h\|_1^2 + \mathscr{C}(\eta_h, \eta_h) &= (u_t - u_{ht}, \mathscr{E}) \\ &\leqslant (\|u_t\|_0 + \|u_{ht}\|_0)\|\mathscr{E}\|_0 \\ &\leqslant ch^2(\|u_t\|_0 + \|u_{ht}\|_0)(\|u\|_2 + \|p\|_1) \end{aligned}$$

Integrating the above inequality from 0 to t and using the Hölder inequality, we have

$$\begin{aligned} &\|u(t) - u_h(t)\|_0^2 + 2\int_0^t (\nu\|e_h\|_1^2 + \mathscr{C}(\eta_h, \eta_h))\,\mathrm{d}s \\ &\leqslant ch^2 \left(\int_0^t (\|u_t\|_0^2 + \|u_{ht}\|_0^2)\,\mathrm{d}s\right)^{1/2} \left(\int_0^t (\|u\|_2^2 + \|p\|_1^2)\,\mathrm{d}s\right)^{1/2} + \|u_0 - u_{0h}\|_0^2 \end{aligned} \tag{29}$$

Applying Theorem 2, Lemmas 2 and 1, we obtain

$$\|u(t) - u_h(t)\|_0^2 + 2\int_0^t (\nu\|e_h\|_1^2 + \mathscr{C}(\eta_h, \eta_h))\,\mathrm{d}s \leqslant ch^2 \tag{30}$$

which, combining with the triangle inequality, (19), (14) and (11), gives (26). □

DOI: 10.1002/fld

Theorem 3
Under the assumptions of Lemma 1 and Theorem 1, the solution (u_h, p_h) of problem (12) and (13) satisfies the following error estimates:

$$\sigma^{1/2}(t)v\|u(t)-u_h(t)\|_1+\sigma(t)(\|u_t(t)-u_{ht}(t)\|_0+\|p(t)-p_h(t)\|_0)\leqslant ch \tag{31}$$

for all $t\in[0,T]$.

Proof
The proof of Theorem 3 consists of Lemmas 4–6. □

Lemma 4
Under the assumptions of Lemma 1 and Theorem 1, the following error estimates hold for $t\in[0,T]$

$$\sigma(t)v\|u(t)-u_h(t)\|_1^2+\int_0^t \sigma(s)\|u_t(s)-u_{ht}(s)\|_0^2\,\mathrm{d}s\leqslant ch^2 \tag{32}$$

Proof
Differentiating the terms $d(e_h,q_h)+\mathscr{C}(\eta_h,q_h)$ in (28) with respect to t and taking $(v_h,q_h)=(e_{ht},\eta_h)$, we get

$$(u_t-u_{ht},e_{ht})+\frac{1}{2}\frac{\mathrm{d}}{\mathrm{d}t}(v\|e_h\|_1^2+\mathscr{C}(\eta_h,\eta_h))=0$$

Noting $e_{ht}=u_t-u_{ht}-\mathscr{E}_t$ and using the Schwarz inequality, we obtain

$$\|u_t-u_{ht}\|_0^2+\frac{\mathrm{d}}{\mathrm{d}t}(v\|e_h\|_1^2+\mathscr{C}(\eta_h,\eta_h))\leqslant\|\mathscr{E}_t\|_0^2$$

Multiplying the above inequality by $\sigma(t)$ and noting

$$0\leqslant\sigma(t)\leqslant 1,\quad \frac{\mathrm{d}}{\mathrm{d}t}\sigma(t)\leqslant 1\quad \forall t\geqslant 0$$

we get

$$\sigma(t)\|u_t-u_{ht}\|_0^2+\frac{\mathrm{d}}{\mathrm{d}t}(\sigma(t)(v\|e_h\|_1^2+\mathscr{C}(\eta_h,\eta_h)))\leqslant v\|e_h\|_1^2+\mathscr{C}(\eta_h,\eta_h)+\sigma(t)\|\mathscr{E}_t\|_0^2 \tag{33}$$

Integrating (33) over $[0,t]$, then combining the triangle inequality with (20) and (30), we complete the proof. □

Lemma 5
Under the assumptions of Lemma 1 and Theorem 1, it holds that, for $t\in[0,T]$

$$\sigma^2(t)\|u_t(t)-u_{ht}(t)\|_0^2+\int_0^t \sigma^2(s)v\|u_t(s)-u_{ht}(s)\|_1^2\,\mathrm{d}s\leqslant ch^2 \tag{34}$$

Proof
Differentiating (28) with respect to t then taking $(v_h,q_h)=(e_{ht},\eta_{ht})$, we find

$$(u_{tt}-u_{htt},e_{ht})+v\|e_{ht}\|_1^2+\mathscr{C}(\eta_{ht},\eta_{ht})=0$$

DOI: 10.1002/fld

Noting that $e_{ht}=u_t-u_{ht}-\mathscr{E}_t$ and using the Schwarz inequality, we deduce

$$\frac{1}{2}\frac{\mathrm{d}}{\mathrm{d}t}\|u_t-u_{ht}\|_0^2+\nu\|e_{ht}\|_1^2+\mathscr{C}(\eta_{ht},\eta_{ht})\leqslant(\|u_{tt}\|_0+\|u_{htt}\|_0)\|\mathscr{E}_t\|_0$$

Multiplying the above inequality by $\sigma^2(t)$, one gets

$$\frac{\mathrm{d}}{\mathrm{d}t}(\sigma^2(t)\|u_t-u_{ht}\|_0^2)+2\sigma^2(t)(\nu\|e_{ht}\|_1^2+\mathscr{C}(\eta_{ht},\eta_{ht}))$$

$$\leqslant 2\sigma(t)\|u_t-u_{ht}\|_0^2+2\sigma^2(t)(\|u_{tt}\|_0+\|u_{htt}\|_0)\|\mathscr{E}_t\|_0$$

Integrating the above inequality from 0 to t, applying Lemma 4 and (20), we obtain

$$\begin{aligned}&\sigma^2(t)\|u_t-u_{ht}\|_0^2+2\int_0^t\sigma^2(s)(\nu\|e_{ht}\|_1^2+\mathscr{C}(\eta_{ht},\eta_{ht}))\,\mathrm{d}s\\&\leqslant 2\int_0^t\sigma(s)\|u_t-u_{ht}\|_0^2\,\mathrm{d}s+c\left(\int_0^t\sigma^2(s)(\|u_{tt}\|_0^2\,\mathrm{d}s+\|u_{htt}\|_0^2)\,\mathrm{d}s\right)^{1/2}\left(\int_0^t\sigma^2(s)\|\mathscr{E}_t\|_0^2\,\mathrm{d}s\right)^{1/2}\\&\leqslant ch^2+ch^2\left(\int_0^t\sigma^2(s)(\|u_{tt}\|_0^2\,\mathrm{d}s+\|u_{htt}\|_0^2)\,\mathrm{d}s\right)^{1/2}\end{aligned}\tag{35}$$

We now estimate $\int_0^t\sigma^2(s)\|u_{htt}\|_0^2\,\mathrm{d}s$. Differentiating (12) with respect to t and then further differentiating the term $d(u_{ht},q_h)+\mathscr{C}(p_{ht},q_h)$ with respect to t, taking $(v_h,q_h)=(u_{htt},p_{ht})$ and using the Schwarz inequality, we get

$$\|u_{htt}\|_0^2+\frac{\mathrm{d}}{\mathrm{d}t}(\nu\|u_{ht}\|_1^2+\mathscr{C}(p_{ht},p_{ht}))\leqslant\|f_t\|_0^2\tag{36}$$

Note that a similar argument for (23) yields

$$\|u_{ht}(t)\|_0^2+\int_0^t(\nu\|u_{ht}\|_1^2+2\mathscr{C}(p_{ht},p_{ht}))\,\mathrm{d}s\leqslant c\tag{37}$$

Multiplying (36) by $\sigma^2(t)$, then integrating it from 0 to t, using (37), (2) and noting $\sigma(t)\leqslant 1$, we find

$$\int_0^t\sigma^2(t)\|u_{htt}\|_0^2\,\mathrm{d}s+\sigma^2(t)(\nu\|u_{ht}\|_1^2+\mathscr{C}(p_{ht},p_{ht}))\leqslant c$$

which, together with (35), (2), the triangle inequality and (20), yields the estimate (34). □

Lemma 6

Under the assumptions of Lemma 1 and Theorem 1, the following estimate holds for $t\in[0,T]$:

$$\sigma(t)\|p(t)-p_h(t)\|_0\leqslant ch\tag{38}$$

DOI: 10.1002/fld

Proof
From (16), (28) and (34), we find

$$\begin{aligned}\sigma(t)\|\eta_h\|_0 &\leqslant \sigma(t)\beta^{-1}\sup_{(v_h,p_h)\in X_h\times M_h}\frac{|\mathscr{B}((e_h,\eta_h);(v_h,q_h))|}{\|v_h\|_1+\|q_h\|_0}\\ &=\sigma(t)\beta^{-1}\sup_{(v_h,q_h)\in X_h\times M_h}\frac{|(u_t-u_{ht},v_h)|}{\|v_h\|_1+\|q_h\|_0}\\ &\leqslant \sigma(t)\beta^{-1}\sup_{(v_h,q_h)\in X_h\times M_h}\frac{C_\Omega\|u_t-u_{ht}\|_0\|v_h\|_1}{\|v_h\|_1+\|q_h\|_0}\\ &\leqslant \beta^{-1}C_\Omega\sigma(t)\|u_t-u_{ht}\|_0\\ &\leqslant ch \end{aligned} \tag{39}$$

Combining (39) with the triangle inequality, (19) and (5), we finish the proof. □

4.3. L^2-error estimates

In order to estimate the error $\|u-u_h\|_0$, we need an auxiliary backward Stokes problem: Find $(\Phi(t),\Psi(t))\in H_0^1(\Omega)^2\times L_0^2(\Omega)$ such that, for $t\in[0,T]$,

$$(v,\Phi_t)-B((v,q);(\Phi,\Psi))=(v,u-u_h)\quad\forall(v,q)\in H_0^1(\Omega)^2\times L_0^2(\Omega),\ \ \Phi(T)=0 \tag{40}$$

This problem is well-posed and has a unique solution (Φ,Ψ) with property [43]:

$$\sup_{0\leqslant t\leqslant T}\|\Phi(t)\|_1^2+\int_0^T(\|\Phi\|_2^2+\|\Psi\|_1^2+\|\Phi_t\|_0^2)\,\mathrm{d}t\leqslant c\int_0^T\|u-u_h\|_0^2\,\mathrm{d}t \tag{41}$$

We introduce the dual Galerkin projection $(\Phi_h(t),\Psi_h(t))$ of $(\Phi(t),\Psi(t))$:

$$\mathscr{B}((v_h,q_h);(\Phi_h,\Psi_h))=B((v_h,q_h);(\Phi,\Psi))\quad\forall(v_h,q_h)\in X_h\times M_h$$

which yields

$$\mathscr{B}((v_h,q_h);(\Phi-\Phi_h,\Psi-\Psi_h))=\mathscr{C}(q_h,\Psi)\quad\forall(v_h,q_h)\in X_h\times M_h \tag{42}$$

A slight modification to the arguments for Lemma 2 (see [29]) yields

$$\|\Phi-\Phi_h\|_0+h(\|\Phi-\Phi_h\|_1+\|\Psi-\Psi_h\|_0)\leqslant ch^2(\|\Phi\|_2+\|\Psi\|_1) \tag{43}$$

Lemma 7
Under the assumptions of Lemma 1 and Theorem 1, the following estimate holds:

$$\int_0^T\mathscr{C}(p_h,p_h)\,\mathrm{d}s\leqslant ch^2 \tag{44}$$

DOI: 10.1002/fld

Proof
Noting that $\mathscr{C}(p_h, p_h)=\mathscr{C}(p-p_h, p-p_h)-\mathscr{C}(p, p)+2\mathscr{C}(p, p_h)$, applying Lemma 3 and combining the Schwarz, Young inequalities with (14), (11) and (5), we see

$$\begin{aligned}\int_0^T \mathscr{C}(p_h, p_h)\,\mathrm{d}s &\leqslant \int_0^T (\mathscr{C}(p-p_h, p-p_h)+\mathscr{C}(p, p))\,\mathrm{d}s+2\int_0^T \mathscr{C}^{1/2}(p, p)\mathscr{C}^{1/2}(p_h, p_h)\,\mathrm{d}s\\ &\leqslant ch^2+2\int_0^T (\mathscr{C}(p, p)+\frac{1}{4}\mathscr{C}(p_h, p_h))\,\mathrm{d}s\\ &\leqslant ch^2+ch^2+\frac{1}{2}\int_0^T \mathscr{C}(p_h, p_h)\,\mathrm{d}s\end{aligned}$$

which yields (44). □

Lemma 8
Under the assumptions of Lemma 1 and Theorem 1, it holds that

$$\int_0^T \|u-u_h\|_0^2\,\mathrm{d}s\leqslant ch^4 \tag{45}$$

Proof
Taking $(v, q)=(e, \eta)=(u-u_h, p-p_h)$ in (40), we get

$$(e, \Phi_t)-B((e, \eta); (\Phi, \Psi))=\|e\|_0^2 \tag{46}$$

Adding (46) and (27) with $(v_h, q_h)=(\Phi_h, \Psi_h)$, noting that $(e, \eta)=(e_h+\mathscr{E}, \eta_h+\mathscr{F})$ and using (42), we obtain

$$\begin{aligned}\|e\|_0^2 &= -\mathscr{B}((e, \eta); (\Phi-\Phi_h, \Psi-\Psi_h))+\mathscr{C}(\eta, \Psi)-\mathscr{C}(p, \Psi_h)+(e, \Phi_t)+(e_t, \Phi_h)\\ &= -\mathscr{C}(\eta_h, \Psi)-\mathscr{B}((\mathscr{E}, \mathscr{F}); (\Phi-\Phi_h, \Psi-\Psi_h))\\ &\quad +\mathscr{C}(p, \Psi-\Psi_h)-\mathscr{C}(p_h, \Psi)+\frac{\mathrm{d}}{\mathrm{d}t}(e, \Phi)-(e_t, \Phi-\Phi_h)\end{aligned}$$

Integrating the above equality from 0 to T, and noting $\Phi(T)=0$, we have

$$\begin{aligned}\int_0^T \|e(s)\|_0^2\,\mathrm{d}s &= -\int_0^T \mathscr{C}(\eta_h, \Psi)\,\mathrm{d}s-\int_0^T \mathscr{B}((\mathscr{E}, \mathscr{F}); (\Phi-\Phi_h, \Psi-\Psi_h))\,\mathrm{d}s+\int_0^T \mathscr{C}(p, \Psi-\Psi_h)\,\mathrm{d}s\\ &\quad -\int_0^T \mathscr{C}(p_h, \Psi)\,\mathrm{d}s-\int_0^T (e_t, \Phi-\Phi_h)\,\mathrm{d}s-(e(0), \Phi(0))\end{aligned} \tag{47}$$

From the Schwarz and Hölder inequalities, (30), (14), (9)–(11) and (41), we have

$$\begin{aligned}\left|\int_0^T \mathscr{C}(\eta_h, \Psi)\,\mathrm{d}s\right| &\leqslant \int_0^T \mathscr{C}^{1/2}(\eta_h, \eta_h)\mathscr{C}^{1/2}(\Psi, \Psi)\,\mathrm{d}s\\ &\leqslant \left(\int_0^T (\mathscr{C}(\eta_h, \eta_h)\,\mathrm{d}s)^{1/2}\left(\int_0^T \mathscr{C}(\Psi, \Psi)\right)\mathrm{d}s\right)^{1/2}\\ &\leqslant ch^2\left(\int_0^T \|\Psi\|_1^2\,\mathrm{d}s\right)^{1/2}\leqslant ch^2\left(\int_0^T \|e(s)\|_0^2\,\mathrm{d}s\right)^{1/2}\end{aligned} \tag{48}$$

DOI: 10.1002/fld

Similarly, applying Lemma 7, Lemma 1, (14), (9)–(11), (41) and (43), one gets

$$\left|\int_0^T \mathscr{C}(p_h,\Psi)\,\mathrm{d}s\right| \leqslant \left(\int_0^T (\mathscr{C}(p_h,p_h)\,\mathrm{d}s\right)^{1/2}\left(\int_0^T \mathscr{C}(\Psi,\Psi))\,\mathrm{d}s\right)^{1/2} \leqslant ch^2\left(\int_0^T \|\Psi\|_1^2\,\mathrm{d}s\right)^{1/2}$$
$$\leqslant ch^2\left(\int_0^T \|e(s)\|_0^2\,\mathrm{d}s\right)^{1/2} \tag{49}$$

$$\left|\int_0^T \mathscr{C}(p,\Psi-\Psi_h)\,\mathrm{d}s\right| \leqslant \left(\int_0^T \mathscr{C}(p,p)\,\mathrm{d}s\right)^{1/2}\left(\int_0^T \mathscr{C}(\Psi-\Psi_h,\Psi-\Psi_h)\,\mathrm{d}s\right)^{1/2}$$
$$\leqslant ch^2\left(\int_0^T \|p\|_1^2\,\mathrm{d}s\right)^{1/2}\left(\int_0^T (\|\Phi\|_2^2+\|\Psi\|_1^2)\,\mathrm{d}s\right)^{1/2}$$
$$\leqslant ch^2\left(\int_0^T \|e(s)\|_0^2\,\mathrm{d}s\right)^{1/2} \tag{50}$$

From (43), (41), (25) and Lemma 1, we see

$$\left|\int_0^T (e_t,\Phi-\Phi_h)\,\mathrm{d}s\right| \leqslant ch^2\int_0^T (\|u_t\|_0+\|u_{ht}\|_0)(\|\Phi\|_2+\|\Psi\|_1)\,\mathrm{d}s$$
$$\leqslant ch^2\left(\int_0^T (\|u_t\|_0^2+\|u_{ht}\|_0^2)\,\mathrm{d}s\right)^{1/2}\left(\int_0^T (\|\Phi\|_2^2+\|\Psi\|_1^2)\,\mathrm{d}s\right)^{1/2}$$
$$\leqslant ch^2\left(\int_0^T \|e(s)\|_0^2\,\mathrm{d}s\right)^{1/2} \tag{51}$$

As for the bilinear term, by applying Theorem 1, Lemma 2, Lemma 1, (41) and (43), we obtain

$$\left|\int_0^T \mathscr{B}((\mathscr{E},\mathscr{F});(\Phi-\Phi_h,\Psi-\Psi_h))\,\mathrm{d}s\right| \leqslant c\int_0^T (\|\mathscr{E}\|_1+\|\mathscr{F}\|_0)(\|\Phi-\Phi_h\|_1+\|\Psi-\Psi_h\|_0)\,\mathrm{d}s$$
$$\leqslant ch^2\int_0^T (\|u\|_2+\|p\|_1)(\|\Phi\|_2+\|\Psi\|_1)\,\mathrm{d}s$$
$$\leqslant ch^2\left(\int_0^T (\|u\|_2^2+\|p\|_1^2)\,\mathrm{d}s\right)^{1/2}\left(\int_0^T (\|\Phi\|_2^2+\|\Psi\|_1^2)\,\mathrm{d}s\right)^{1/2}$$
$$\leqslant ch^2\left(\int_0^T \|e(s)\|_0^2\,\mathrm{d}s\right)^{1/2} \tag{52}$$

In addition, by the definition of u_{0h} and (41), we have

$$|e(0),\Phi(0)| = |(u_0-R_h(u_0,p_0),\Phi(0))| \leqslant ch^2\|\Phi(0)\|_1 \leqslant ch^2\left(\int_0^T \|e(s)\|_0^2\,\mathrm{d}s\right)^{1/2} \tag{53}$$

Combining (47) with (48)–(53), we complete the proof of (45). □

DOI: 10.1002/fld

Theorem 4
Under the assumptions of Lemma 1 and Theorem 1, it holds that, for $t \in [0, T]$,

$$\sigma^{1/2}(t)\|u(t)-u_h(t)\|_0 \leqslant ch^2 \tag{54}$$

Proof
Taking $(v_h, q_h)=(e_h, \eta_h)$ in (28), we see

$$\frac{1}{2}\frac{\mathrm{d}}{\mathrm{d}t}\|e_h\|_0^2+\nu\|e_h\|_1^2+\mathscr{C}(\eta_h, \eta_h)\leqslant\|\mathscr{E}_t\|_0\|e_h\|_0 \tag{55}$$

Note that from (20), Lemmas 8, 2 and (5), we have

$$\int_0^t \sigma(t)\|\mathscr{E}_t\|_0^2\,\mathrm{d}s \leqslant ch^4 \tag{56}$$

$$\int_0^t \|e_h\|_0^2 \leqslant 2\int_0^T (\|u-u_h\|_0^2+\|\mathscr{E}\|_0^2)\,\mathrm{d}s \leqslant ch^4 \tag{57}$$

$$\|u_0-u_{0h}\|_0=\|u_0-R(u_0, p_0)\|_0 \leqslant ch^2 \tag{58}$$

Multiplying (55) by $\sigma(t)$ then integrating it from 0 to t, using (56)–(58) gives

$$\sigma(t)\|e_h\|_0^2+2\int_0^T \sigma(t)(\nu\|e_h\|_1^2+\mathscr{C}(\eta_h, \eta_h))\,\mathrm{d}s \leqslant ch^4 \tag{59}$$

Combining the triangle inequality with (59) and (20), we finish the proof. □

5. NUMERICAL RESULTS

In this section, we present two series of numerical results to illustrate the theoretical analysis of the new stabilized method for the time-dependent Stokes problem. For comparison, we also give the numerical results for the P_1-P_1 element using the stabilization technique proposed in [33] and the results for the stable MINI element. In all experiments, Ω is the unit square $[0, 1]\times[0, 1]$ in R^2. The mesh consists of triangular elements that are obtained by dividing Ω into sub-squares of equal size and then drawing the diagonal in each sub-square; see Figure 1. The viscosity is set as $\nu=1.0$. The projection operator Π, which stabilizes the lowest-order conforming P_1-P_0 element, is the Clément interpolant satisfying (9)–(11) (see [41]). The definition of Π_0 (see [33] for detailed information), which stabilizes the lowest equal-order P_1-P_1 element is a standard local L^2 projection operator:

$$\Pi_0 q|_K=\frac{1}{\mathrm{Meas}(K)}\int_K q\,\mathrm{d}x \quad \forall K\in T^h(\Omega),\ \ q\in L^2(\Omega)$$

which also satisfies the properties (9)–(11) [41]. The software Freefem++ developed by Hecht *et al.* [44] is used in our experiments. We also use the UMFPACK routine [45] to solve the linear systems arising at each time step both in Examples 1 and 2.

DOI: 10.1002/fld

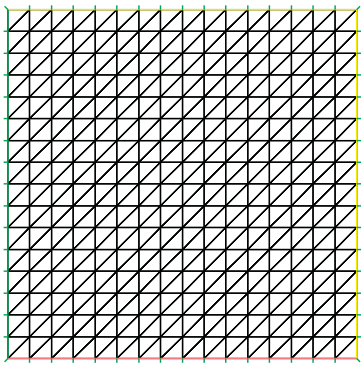

Figure 1. Uniform triangulation of Ω into triangles.

5.1. *Analytical solution*

In this test, we perform one step of the implicit Euler method with time step size $\Delta t = 0.005$ for the exact solution

$$u_1 = \pi \sin^2(\pi x) \sin(2\pi y) \cos(t)$$

$$u_2 = -\pi \sin(2\pi x) \sin^2(\pi y) \cos(t)$$

$$p = 10 \cos(\pi x) \cos(\pi y) \cos(t)$$

The initial condition in (1) is set equal to the exact solution and f is computed by evaluating the momentum equation of problem (1) for the exact solution.

Results for the new stabilized $P_1 - P_0$, $P_1 - P_1$ and MIN elements are shown in Tables I–III, respectively, in which

$$K_{\text{div}} = \max_{K \in T^h(\Omega)} \left| \int_K \text{div}\, u_h \, \text{d}x \right|$$

The experimental rates of convergence with respect to the mesh size h are calculated by the formula $\log(E_i/E_{i+1})/\log(h_i/h_{i+1})$, where E_i and E_{i+1} are the relative errors corresponding to the meshes of size h_i and h_{i+1}, respectively. In our numerical results, there is not much difference in H^1-errors of the velocity among the three methods. However, as shown in Tables I, II and III, the difference is big in L^2-errors of the velocity. The L^2-errors of the velocity both obtained by the new stabilized $P_1 - P_0$ and $P_1 - P_1$ elements are bigger than that of the velocity computed by MIN element, while the accuracy in L^2-norm of the velocity computed by stabilized $P_1 - P_1$ element is higher than that of the stabilized $P_1 - P_0$ element; see Figure 2(a) and (b). A large difference is observed among the three methods for the pressure approximation in accuracy and convergence rates. Both the stabilized $P_1 - P_1$ element and the stable MINI element show a superconvergence behavior for the pressure approximation; the former is better than the latter in terms of accuracy and convergence rate; see Figure 2(c). Between the stabilized $P_1 - P_0$ and $P_1 - P_1$ elements, the $P_1 - P_1$ element shows a better accuracy in L^2-norm both for the velocity and pressure. An interesting find is that the stabilized $P_1 - P_0$ element has smaller K_{div} values than MINI element whose K_{div} values, in turn, are smaller than that of the stabilized $P_1 - P_1$ element.

DOI: 10.1002/fld

Table I. Finite element errors after one implicit Euler step: new stabilized $P_1 - P_0$ element.

$1/h$	$\frac{\|u-u_h\|_{0,\Omega}}{\|u\|_{0,\Omega}}$	$\frac{\|u-u_h\|_{1,\Omega}}{\|u\|_{1,\Omega}}$	$\frac{\|p-p_h\|_{0,\Omega}}{\|p\|_{0,\Omega}}$	K_{div}	u_{L^2} rate	u_{H^1} rate	p_{L^2} rate
10	0.0730941	0.252504	0.576377	0.0167081			
20	0.0188265	0.127949	0.253199	0.00233646	1.95699	0.980734	1.18674
30	0.00841335	0.0854539	0.160507	0.000699486	1.98648	0.995538	1.12424
40	0.00474356	0.0641217	0.117702	0.000296267	1.99189	0.998301	1.07819
50	0.00304085	0.0513063	0.0930414	0.00015184	1.99267	0.999221	1.05365
60	0.0021149	0.0427582	0.0769787	8.79014e−005	1.99169	0.999619	1.03946
70	0.00155627	0.0366509	0.0656717	5.53715e−005	1.98973	0.999819	1.03055
80	0.00119358	0.0320699	0.0572745	3.70899e−005	1.98707	0.99993	1.02457
90	0.000944868	0.0285066	0.0507888	2.60541e−005	1.98385	0.999995	1.02035
100	0.000766948	0.0256558	0.0456269	1.89894e−005	1.98012	1.00003	1.01724

Table II. Finite element errors after one implicit Euler step: new stabilized $P_1 - P_1$ element.

$1/h$	$\frac{\|u-u_h\|_{0,\Omega}}{\|u\|_{0,\Omega}}$	$\frac{\|u-u_h\|_{1,\Omega}}{\|u\|_{1,\Omega}}$	$\frac{\|p-p_h\|_{0,\Omega}}{\|p\|_{0,\Omega}}$	K_{div}	u_{L^2} rate	u_{H^1} rate	p_{L^2} rate
10	0.0669041	0.252863	0.31111	0.017304			
20	0.0171354	0.12803	0.0916053	0.0023884	1.96511	0.981875	1.76392
30	0.00765053	0.0854892	0.0432043	0.000716096	1.98876	0.99608	1.85355
40	0.00431236	0.0641416	0.0253648	0.000303123	1.99279	0.998659	1.85128
50	0.0027643	0.0513191	0.0168382	0.000155452	1.99289	0.999493	1.83608
60	0.00192265	0.0427672	0.0120858	8.9977e−005	1.99142	0.999841	1.81889
70	0.00141495	0.0366575	0.00915423	5.66965e−005	1.98903	1.00001	1.80221
80	0.00108536	0.0320749	0.0072112	3.79739e−005	1.98595	1.00009	1.78669
90	0.000859359	0.0285106	0.0058525	2.668e−005	1.98227	1.00014	1.77246
100	0.000697692	0.0256591	0.0048622	1.94444e−005	1.97806	1.00016	1.75947

Table III. Finite element errors after one implicit Euler step: stable MINI element.

$1/h$	$\frac{\|u-u_h\|_{0,\Omega}}{\|u\|_{0,\Omega}}$	$\frac{\|u-u_h\|_{1,\Omega}}{\|u\|_{1,\Omega}}$	$\frac{\|p-p_h\|_{0,\Omega}}{\|p\|_{0,\Omega}}$	K_{div}	u_{L^2} rate	u_{H^1} rate	p_{L^2} rate
10	0.0419119	0.243917	0.352077	0.0177416			
20	0.0103905	0.121541	0.0988782	0.00238496	2.0121	1.00495	1.83217
30	0.00460743	0.0808947	0.0499966	0.000706559	2.00564	1.00405	1.68186
40	0.00259091	0.0606146	0.0313927	0.000297343	2.00104	1.00324	1.61768
50	0.00165931	0.0484626	0.022038	0.000152424	1.99694	1.00269	1.58557
60	0.00115384	0.0403687	0.0165612	8.82874e−005	1.99266	1.00229	1.56703
70	0.000849298	0.0345911	0.0130311	5.56103e−005	1.98794	1.00199	1.55513
80	0.00065175	0.03026	0.0105992	3.72626e−005	1.98267	1.00177	1.54688
90	0.000516372	0.0268928	0.00884008	2.61743e−005	1.9768	1.00158	1.54084
100	0.000419572	0.0241999	0.00751905	1.90839e−005	1.9703	1.00144	1.53621

The numerical results support our theoretical results and show that the new stabilized method is highly efficient for the time-dependent Stokes problem. It takes less CPU time than the stable MINI element; see Table IV. Especially, the stabilized $P_1 - P_1$ element has a better performance

DOI: 10.1002/fld

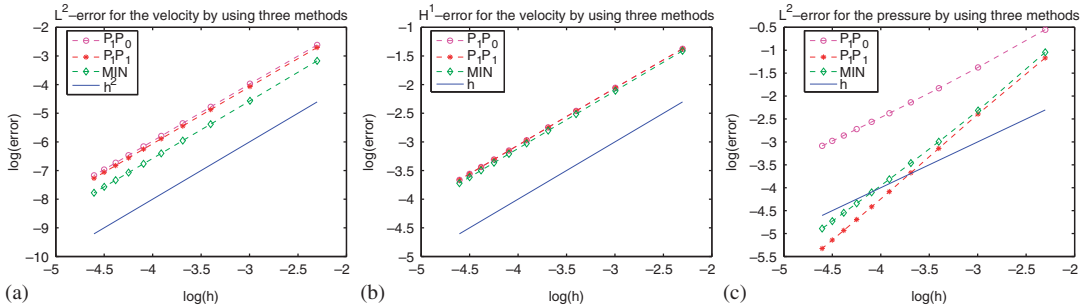

Figure 2. Error of Example 1: (a) L^2-error for the velocity; (b) H^1-error for the velocity; and (c) L^2-error for the pressure.

Table IV. CPU time in seconds of Example 1 by using three methods: one implicit Euler step.

$1/h$	10	20	30	40	50	60	70	80	90	100
P_1-P_0	0.187	0.484	1.094	1.938	3.11	4.531	6.187	8.266	10.672	13.266
P_1-P_1	0.188	0.469	1.078	1.906	3.078	4.484	6.11	8.14	10.609	13.203
MIN	0.219	0.515	1.234	2.125	3.391	4.922	6.766	8.937	11.625	14.562

than the stable MINI element both in terms of accuracy and convergence rate for the pressure approximation.

5.2. *Lid-driven cavity problem*

For this test, we consider the incompressible lid-driven cavity flow problem defined on the unit square. The flow domain and the boundary conditions are shown in Figure 3. The initial condition is taken as $u_0=0$. The mesh consists of triangular elements and the mesh size $h=\frac{1}{60}$. The implicit backward Euler scheme is also used for the time discretization with time step size $\Delta t=0.01$.

Figures 4 and 5 depict the velocity vectors and the pressure contours, respectively, at the steady state by using the three different mixed finite elements, where the stopping criterion

$$\frac{\|u_h^{n+1}-u_h^n\|_{0,\Omega}}{\|u_h^{n+1}\|_{0,\Omega}}\leqslant 10^{-6} \tag{60}$$

is employed. Here u_h^{n+1} is the approximation of $u_h(t)$ at time $t=(n+1)\Delta t$. As in Example 1, we observe that the difference in velocity among the three methods is small, while that of the pressure is big.

Table V reports the CPU time needed to reach the steady state for the new stabilized P_1-P_0, P_1-P_1 and MIN elements with different time step sizes, where the number in parentheses denotes the time steps count satisfying the stopping criterion (60). In Table VI, we also list the values of $p_h(1,1)-p_h(0,1)$ at the steady state to test how well the singularity of the problem is approached by the three mixed elements. It is observed that the three methods have the same convergence speed in terms of the time steps satisfying the stopping criterion. However, the new stabilized

DOI: 10.1002/fld

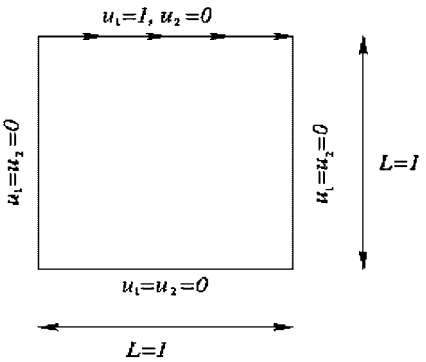

Figure 3. Lid-driven cavity flow.

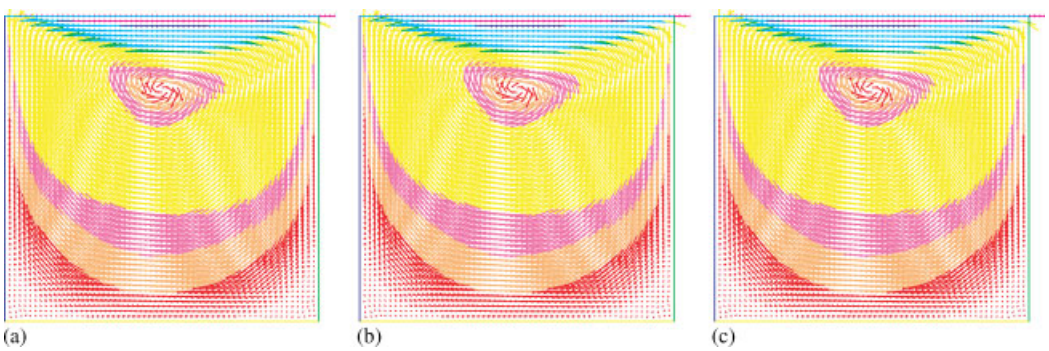

Figure 4. Velocity vectors of the driven cavity flow at the steady state: (a) $P_1 - P_0$ element; (b) $P_1 - P_1$ element; and (c) MIN element.

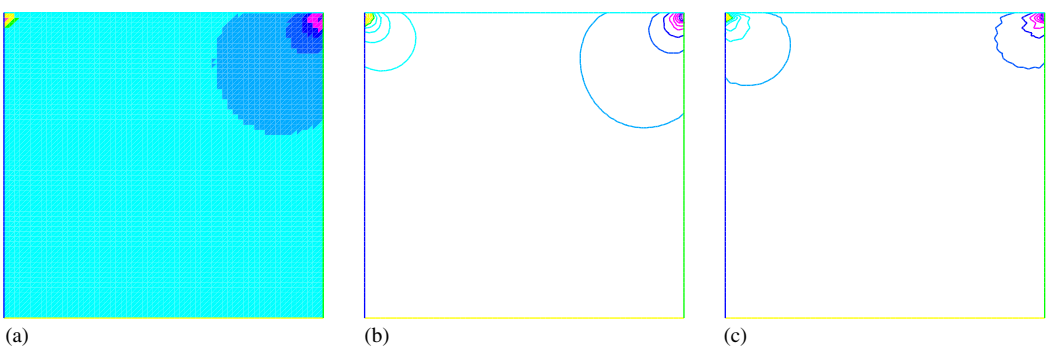

Figure 5. Pressure contours of the driven cavity flow at the steady state: (a) $P_1 - P_0$ element; (b) $P_1 - P_1$ element; and (c) MIN element.

DOI: 10.1002/fld

Table V. CPU time in seconds needed to reach a steady state for the lid-driven cavity problem.

Δt	0.5	0.1	0.05	0.01	0.005	0.001
P_1-P_0	13.641 (5)	21.406 (8)	29.469 (11)	79.375 (30)	132.703 (50)	518.735 (196)
P_1-P_1	13.469 (5)	21.140 (8)	29.094 (11)	79.063 (30)	131.718 (50)	517.234 (196)
MINI	14.016 (5)	22.390 (8)	30.922 (11)	83.969 (30)	140.000 (50)	547.797 (196)

Table VI. Pressure singularity at the steady state as functions of Δt for the lid-driven cavity problem.

Δt	0.5	0.1	0.05	0.01	0.005	0.001
P_1-P_0	168.796	168.796	168.796	168.796	168.796	168.796
P_1-P_1	200.542	200.542	200.542	200.542	200.542	200.542
MINI	238.544	238.544	238.544	238.544	238.544	238.544

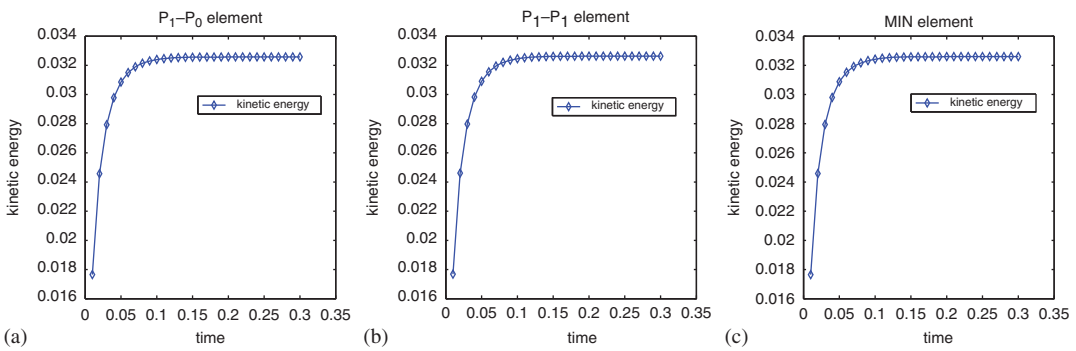

Figure 6. Evolution of the kinetic energy in time for the lid-driven cavity flow: (a) P_1-P_0 element; (b) P_1-P_1 element; and (c) MIN element.

P_1-P_0 and P_1-P_1 elements take less CPU time than the MIN element. On the other hand, we see from Table VI that the MIN element captures the pressure singularity better than the stabilized P_1-P_0 and P_1-P_1 elements. In Figure 6, we plot the evolution of the kinetic energy $\|u_h^{n+1}\|_{0,\Omega}^2/2$ using $\Delta t=0.01$ until it reaches its steady state, where we observe the fast convergence toward the steady state and the absence of oscillations along the process.

6. CONCLUSIONS

In this paper, we have provided a theoretical analysis for a new stabilized finite element method based on pressure projection in the context of the P_1-P_0 triangular element and the Q_1-P_0 quadrilateral element. The analysis has extended the work in [33, 34] for the stationary Stokes equations to the time-dependent Stokes problem. Numerical results support the theoretical results

DOI: 10.1002/fld

and show that the new stabilized method, successfully applied to the stationary Stokes problem, is also highly efficient for the non-stationary Stokes problem. Compared with the stable MINI element, it is simpler and takes less CPU time. Between the new stabilized elements, the stabilized $P_1 - P_1$ element shows a better performance than the stabilized $P_1 - P_0$ element in terms of the accuracy of the approximate solution. The stabilized $P_1 - P_1$ element also has a better performance than the stable MINI element both in terms of accuracy and convergence rate for the pressure approximation.

ACKNOWLEDGEMENTS

The author would like to thank the editor and the referees for their valuable comments and suggestions that helped to improve the results of this paper.

REFERENCES

1. Brooks A, Hughes T. Streamline upwind/Petrov–Galerkin formulations for convection dominated flows with particular emphasis on the incompressible Navier–Stokes equations. *Computer Methods in Applied Mechanics and Engineering* 1982; **32**(1–3):199–259.
2. Hughes T, Franca L, Balestra M. A new finite element formulation for computational fluid dynamics: V. Circumventing the Babuska–Brezzi condition: a stable Petrov–Galerkin formulation of the Stokes problem accommodating equal-order interpolations. *Computer Methods in Applied Mechanics and Engineering* 1986; **59**(1):85–99.
3. Brezzi F, Pitkaranta J. On the stabilization of finite element approximations of the Stokes problem. In *Efficient Solution of Elliptic Systems*, Hackbush W (ed.). Notes on Numerical Fluid Mechanics, vol. 10. Friedr. Vieweg & Sohn: Braunschweig, 1984.
4. Douglas J, Wang J. An absolutely stabilized finite element method for the Stokes problem. *Mathematics of Computation* 1989; **52**:495–508.
5. Franca L, Frey F. Stabilized finite element methods: II. The incompressible Navier–Stokes equations. *Computer Methods in Applied Mechanics and Engineering* 1992; **99**(2–3):209–233.
6. Franca L, Hughes T. Convergence analyses of Galerkin-least-squares methods for symmetric advective–diffusive forms of the Stokes and incompressible Navier–Stokes equations. *Computer Methods in Applied Mechanics and Engineering* 1993; **105**(2):285–298.
7. Franca L, Stenberg R. Error analysis of some Galerkin least squares methods for the elasticity equations. *SIAM Journal on Numerical Analysis* 1991; **28**(6):1680–1697.
8. Baiocchi C, Brezzi F, Franca L. Virtual bubbles and Galerkin-least–squares type methods (Ga. L.S.). *Computer Methods in Applied Mechanics and Engineering* 1993; **105**(1):125–141.
9. Brezzi F, Bristeau M, Franca L, Mallet M, Rogé G. A relationship between stabilized finite element methods and the Galerkin method with bubble functions. *Computer Methods in Applied Mechanics and Engineering* 1992; **96**(1):117–129.
10. Barrenechea GR, Valentin F. An unusual stabilized finite element method for a generalized Stokes problem. *Numerische Mathematik* 2002; **92**(4):653–677.
11. Araya R, Barrenechea GR, Valentin F. Stabilized finite element methods based on multiscaled enrichment for the Stokes problem. *SIAM Journal on Numerical Analysis* 2006; **44**(1):322–348.
12. Barrenechea GR, Valentin F. Relationship between multiscale enrichment and stabilized finite element methods for the generalized Stokes problem. *Comptes Rendus Mathematique* 2005; **341**(10):635–640.
13. Barth T, Bochev P, Gunzburger M, Shahid J. A taxonomy of consistently stabilized finite element methods for the Stokes problem. *SIAM Journal on Scientific Computing* 2004; **25**(5):1585–1607.
14. Codina R, Blasco J. A finite element formulation for the Stokes problem allowing equal velocity–pressure interpolation. *Computer Methods in Applied Mechanics and Engineering* 1997; **143**(3–4):373–391.
15. Codina R, Blasco J. Analysis of a pressure-stabilized finite element approximation of the stationary Navier–Stokes equations. *Numerische Mathematik* 2000; **87**(1):59–81.

DOI: 10.1002/fld

16. Codina R, Blasco J, Buscaglia G, Huerta A. Implementation of a stabilized finite element formulation for the incompressible Navier–Stokes equations based on a pressure gradient projection. *International Journal for Numerical Methods in Fluids* 2001; **37**(4):419–444.
17. Becker R, Braack M. A finite element pressure gradient stabilization for the Stokes equations based on local projections. *Calcolo* 2001; **38**(4):173–199.
18. Silvester DJ. Optimal low-order finite element methods for incompressible flow. *Computer Methods in Applied Mechanics and Engineering* 1994; **111**(3–4):357–368.
19. Silvester DJ. Stabilized mixed finite element methods. *Numerical Analysis Report No. 262*, Department of Mathematics, University of Manchester Institute of Science and Technology, Manchester, U.K., 1995.
20. Silvester DJ, Kechkar N. Stabilized bilinear-constant velocity–pressure finite elements for the conjugate gradient solution of the Stokes problem. *Computer Methods in Applied Mechanics and Engineering* 1990; **79**(10):71–86.
21. Choi HG, Choi H, Yoo JY. A fractional four-step finite element formulation of the unsteady incompressible Navier–Stokes equations using SUPG and linear equal-order element methods. *Computer Methods in Applied Mechanics and Engineering* 1997; **143**(3–4):333–348.
22. Tezduyar T, Mittal S, Shih R. Time-accurate incompressible flow computations with quadrilateral velocity–pressure elements. *Computer Methods in Applied Mechanics and Engineering* 1991; **87**(2–3):363–384.
23. Codina R, Zienkiewicz OC. CBS versus GLS stabilization of the incompressible Navier–Stokes equations and the role of the time step as stabilization parameter. *Communications in Numerical Methods in Engineering* 2002; **18**(2):99–112.
24. Picasso M, Rappaz J. Stability of time-splitting schemes for the Stokes problem with stabilized finite elements. *Numerical Methods for Partial Differential Equations* 2001; **17**(6):632–656.
25. Bochev P, Gunzburger M, Shadid J. On inf–sup stabilized finite element methods for transient problems. *Computer Methods in Applied Mechanics and Engineering* 2004; **193**(15–16):1471–1489.
26. Barrenechea GR, Blasco J. Pressure stabilization of finite element approximations of time-dependent incompressible flow problems. *Computer Methods in Applied Mechanics and Engineering* 2007; **197**:219–231.
27. He Y. A fully discrete stabilized finite-element method for the timedependent Navier–Stokes problem. *IMA Journal of Numerical Analysis* 2003; **23**:665–691.
28. He Y, Sun W. Stabilized finite element method based on the Crank–Nicolson extrapolation scheme for the time-dependent Navier–Stokes equations. *Mathematics of Computation* 2007; **76**(257):115–136.
29. Li J, He Y, Chen Z. A new stabilized finite element method for the transient Navier–Stokes equations. *Computer Methods in Applied Mechanics and Engineering* 2007; **197**(1):22–35.
30. Blasco J, Codina R. Space and time error estimates for a first order, pressure stabilized finite element method for the incompressible Navier–Stokes equations. *Applied Numerical Mathematics* 2001; **38**(4):475–497.
31. Codina R, Blasco J. Stabilized finite element method for the transient Navier–Stokes equations based on a pressure gradient projection. *Computer Methods in Applied Mechanics and Engineering* 2000; **182**(3–4):277–300.
32. Li J, Mei L, He Y. A pressure-Poisson stabilized finite element method for the non-stationary Stokes equations to circumvent the inf–sup condition. *Applied Mathematics and Computation* 2006; **182**(1):24–35.
33. Bochev P, Dohrmann C, Gunzburger M. Stabilization of low-order mixed finite elements for the Stokes equations. *SIAM Journal on Numerical Analysis* 2006; **44**(1):82–101.
34. Dohrmann C, Bochev P. A stabilized finite element method for the Stokes problem based on polynomial pressure projections. *International Journal for Numerical Methods in Fluids* 2004; **46**(2):183–201.
35. Li J, He Y. A stabilized finite element method based on two local Gauss integrations for the Stokes equations. *Journal of Computational and Applied Mathematics* 2008; **214**(1):58–65.
36. He Y, Li J. A stabilized finite element method based on local polynomial pressure projection for the stationary Navier–Stokes equations. *Applied Numerical Mathematics* 2008; **58**(10):1503–1514.
37. Adams R. *Sobolev Spaces*. Academic Press Inc.: New York, 1975.
38. Ciarlet PG, Lions JL. *Handbook of Numerical Analysis*, *Vol. II*, *Finite Element Methods* (*Part I*). Elsevier Science Publisher: Amsterdam, 1991.
39. Heywood JG, Rannacher R. Finite element approximation of the nonstationary Navier–Stokes problem I: regularity of solutions and second-order error estimates for spatial discretization. *SIAM Journal on Numerical Analysis* 1982; **19**(2):275–311.
40. Ciarlet PG. *The Finite Element Method for Elliptic Problems*. North-Holland: Amsterdam, 1978.
41. Girault V, Raviart PA. *Finite Element Method for Navier–Stokes Equations*: *Theory and Algorithms*. Springer: Berlin, Heidelberg, 1987.

DOI: 10.1002/fld

42. Sani RL, Gresho PM, Lee RL, Griffiths DF. The cause and cure(?) of the spuious pressure generated by certain finite element method solutions of the incompressible Navier–Stokes equations, Part 1 and Part 2. *International Journal for Numerical Methods in Fluids* 1981; **1**(1):17–43; **1**(2):171–204.
43. Hill AT, Süli E. Approximation of the global attractor for the incompressible Navier–Stokes equations. *IMA Journal of Numerical Analysis* 2000; **20**:633–667.
44. Hecht F, Pironneau O, Le Hyaric A, Ohtsuka K. Available at: http://www.freefem.org/ff++ [6 May 2008].
45. Davis TA. Available at: http://www.cise.ufl.edu/research/sparse/umfpack [6 May 2008].

DOI: 10.1002/fld